Anderson transition: a novel route to high thermoelectric performance

Fabian Garmroudi (fabian.garmroudi@tuwien.ac.at)
TU Wien https://orcid.org/0000-0002-0088-1755
Michael Parzer
Technische Universität Wien
Alexander Riss
Technische Universität Wien https://orcid.org/0000-0002-9707-8394
Andrei Ruban
KTH Royal Institute of Technology
Sergii Khmelevskyi
Technische Universität Wien
Michele Reticcioli
Universität Wien https://orcid.org/0000-0001-8223-9928
Matthias Knopf
Technische Universität Wien
Herwig Michor
Technische Universität Wien https://orcid.org/0000-0003-1642-5946
Andrej Pustogow
Technische Universität Wien
Takao Mori
National Institute for Materials Science https://orcid.org/0000-0003-2682-1846
Ernst Bauer
Technische Universität Wien

Physical Sciences - Article

Keywords: thermoelectricity, energy efficiency, Anderson transition

Posted Date: September 27th, 2021

DOI: https://doi.org/10.21203/rs.3.rs-929834/v1

Version of Record: A version of this preprint was published at Nature Communications on June 23rd, 2022. See the published version at https://doi.org/10.1038/s41467-022-31159-w.

Anderson transition: a novel route to high thermoelectric performance

Fabian Garmroudi[a], **Michael Parzer**[a], **Alexander Riss**[a], **Andrei V. Ruban**[b,c], **Sergii Khmelevskyi**[d], **Michele Reticcioli**[e], **Matthias Knopf**[a], **Herwig Michor**[a], **Andrej Pustogow**[a], **Takao Mori**[f,g], **Ernst Bauer**[a]

[a] *Institute of Solid State Physics, Technische Universität Wien, Vienna, Austria*
[b] *Department of Materials Science and Engineering, KTH Royal Institute of Technology, Stockholm, Sweden*
[c] *Materials Center Leoben Forschung GmbH, Leoben, Austria*
[d] *Research Center for the Computational Materials Science and Engineering, Technische Universität Wien, Vienna, Austria*
[e] *Faculty of Physics, Center for Computational Materials Science, Universität Wien, Vienna, Austria*
[f] *International Center for Materials Nanoarchitectonics (WPI-MANA), National Institute for Materials Science, Tsukuba, Japan*
[g] *Graduate School of Pure and Applied Sciences, University of Tsukuba, Tsukuba, Japan*

Discovered exactly 200 years ago in 1821,[1] thermoelectricity is nowadays of global interest as it allows to directly interconvert thermal and electrical energy via the Seebeck/Peltier effect, which could be exploited to enhance energy efficiency[2,3]. In their seminal work[4], Mahan and Sofo mathematically derived the conditions for 'the best thermoelectric' – a delta-distribution-shaped electronic transport function, where charge carriers contribute to transport only in an infinitely narrow energy interval. So far, however, only approximations to this concept were expected to really exist in nature[4,5]. Here, we propose as a physical realisation of this scenario the Anderson transition in an impurity band, i.e. the transition from Anderson-localised to extended quantum states[6]. We obtained a significant enhancement and dramatic change of the thermoelectric properties from p-type to n-type in the stoichiometric Heusler compound Fe_2VAl, which we assign to a narrow region of delocalised electrons in the energy spectrum near the Fermi energy. We achieved this through an innovative approach of driving the Anderson transition via continuous disorder tuning: variable amounts of atomic defects are induced in a controlled fashion by thermal quenching from high temperatures ($950 - 1380\,^{\circ}C$). Based on our experimental electronic transport and magnetisation results, supported by Monte-Carlo and density functional theory calculations, we demonstrate a universal enhancement strategy towards colossal thermoelectric performance that is applicable to diverse material classes.

Thermoelectric (TE) devices are capable of converting wasted heat into useful electrical energy or act as Peltier coolers. Facing an increasing worldwide demand for efficient energy utilisation, the immense diversity of potential technologocial applications has sparked great interest[2,3]. Still, TE devices are currently restrained in their applicability due to their limited efficiency. The dimensionless figure of merit $ZT = S^2\sigma T/(\kappa_e + \kappa_{ph})$, which is closely related to the conversion efficiency, comprises three material-dependent parameters. These are the thermopower S, the electrical conductivity σ and the thermal conductivity κ, consisting of a contribution from electrons κ_e and phonons κ_{ph}, which are the quanta of lattice vibrations. While considerable progress towards achieving high ZT has been achieved so far by reducing κ_{ph}[7,8], increasing the electronic part of ZT is a much more formidable, yet necessary task and new exotic concepts for enhancement are required. In 1996, Mahan and Sofo mathematically identified 'the best thermoelectric' as an ideal system, characterised by an infinitely narrow delta-distribution-shaped transport function $\Sigma(E)$[4].

Here, we propose that this seemingly unrealisable mathematical concept becomes actually realised in real materials at the Anderson transition in an impurity band, as predicted theoretically[9]. As sketched in Fig.1, such a transition occurs when the number of randomly distributed impurities increases above a critical value x_c, known as quantum percolation. Below x_c, all impurity states are Anderson-localised due to disorder[10]. A singularity of the transport function occurs at x_c when an infinitesimally small region of states in the density of states (DOS) becomes delocalised. This was explained by Mott in 1967 through the concept of 'mobility edges', which are two critical energies $E_{c_{1,2}}$ that appear at the centre of an impurity band, separating localised states in the band tails from delocalised, extended states in the centre[11]. Far above x_c, E_{c_1} and E_{c_2} shift towards the band edges, eventually delocalising all impurity states.

Our study is focused on the TE transport properties across the Anderson transition in an impurity band with

*Corresponding author

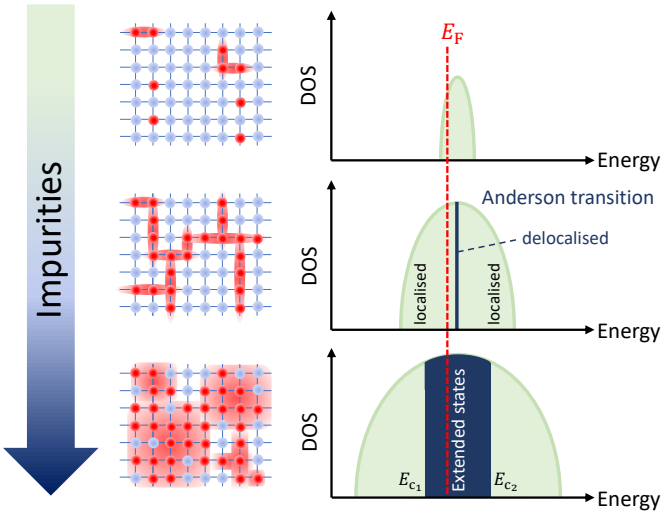

Fig. 1: Schematic of the Anderson transition in an impurity band with increasing impurity concentration. When the number of randomly distributed impurities in a peridocally ordered crystal increases, the impurity electrons remain localised below a threshold value due to Anderson localisation. At the Anderson transition, the critical density of impurities allows for delocalisation of an infinitely narrow energy region of extended states inside the localised impurity states. The delocalised impurity band is marked by two mobility edges $E_{c_{1,2}}$, which are critical energies that separate the localised from delocalised states.

two mobility edges. We experimentally realised such a scenario in undoped, stoichiometric bulk Fe_2VAl by controlling the degree of lattice disorder via thermal quenching. This Heusler compound recently became an excellent candidate for studying new TE optimisation strategies[12–14]. Our measurements of the electronic transport and magnetisation in this work, supported by Monte-Carlo and density functional theory (DFT) simulations, show clear evidence for a significant enhancement of the TE performance, which we attribute to the Anderson transition. In the following, we describe the structural, electronic and magnetic properties of disorder-tuned Fe_2VAl as obtained by our experiments and simulations; finally, we show the TE properties of the material at the Anderson transition.

Structural and electronic properties

Ternary Fe_2VAl forms a fully ordered $L2_1$ structure at low temperatures that undergoes two second-order structural phase transitions (see Fig.2a) into the partly disordered B2 structure at $T_{B2} \approx 1100\,^{\circ}C$ and fully disordered A2 structure at $T_{A2} \approx 1250\,^{\circ}C$[15]. Our Monte-Carlo simulations based on effective cluster interactions show how the degree of atomic disorder in bulk Fe_2VAl can be controlled by temperature, finding a remarkable agreement with the experimental $L2_1-B2$ transition temperature[15] (the $B2-A2$ transition temperature was overestimated as dicussed in Methods). This allows us to semiquantitatively assess the concentration of Fe, V and Al atoms on the respective sublattices as depicted in Fig.2b. Note that while the V/Al sublattice is fully disordered in the B2 phase, there is already a significant site exchange on the Fe sublattice (5–25 % Fe antisites). The large amount of antisite defects obtained at high temperatures as a result of the thermal excitations can be partly frozen by ultrafast quenching our samples.

To illustrate the nature of localised Fe/V antisite electronic states near the Fermi energy E_F, we calculated the spin-polarised DOS by making use of the exact muffin-tin orbital coherent potential approximation method (EMTO-CPA). This method allows to calculate the DOS of a single-impurity embedded in an infinitely large and ordered effective medium, mimicking the electronic and structural properties of an alloy in the dilute limit of antisite concentration $x_{AS} \to 0$. Figs.2c,d show the occurence of sharp, hydrogen-like impurity states near E_F for both Fe_V and V_{Fe} defects, as compared to the fully ordered compound. Similar results are obtained for Fe_{Al} impurity states (see Extended Data Fig.2). Furthermore, the spin degeneracy

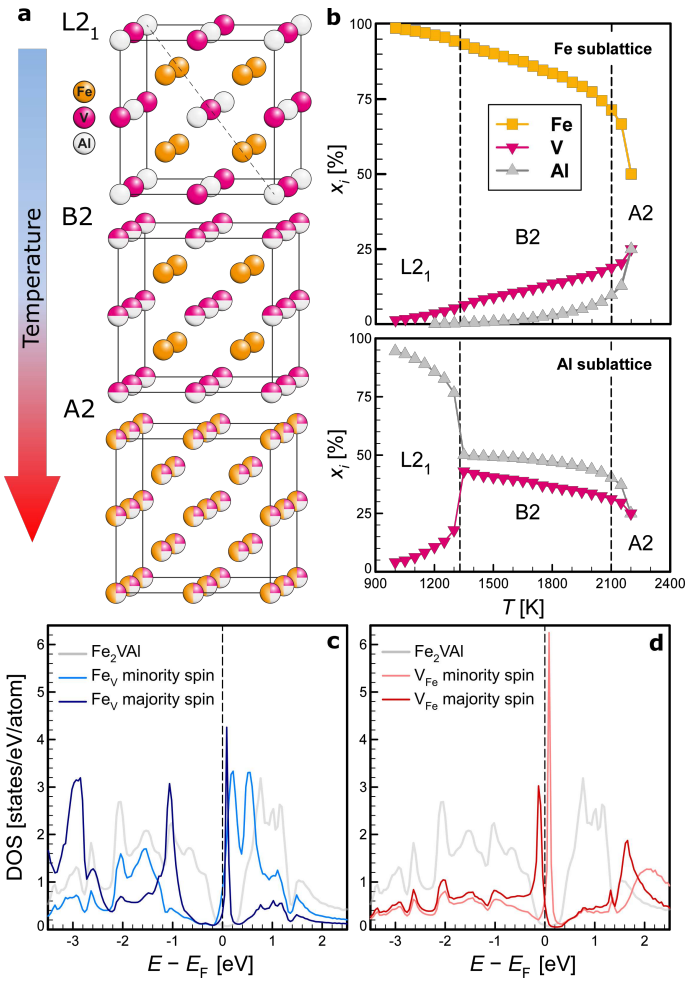

Fig. 2: **a**, Order-disorder transitions in Fe_2VAl occuring at high temperatures. **b**, Monte-Carlo-simulated concentrations of site occupancies in the $L2_1$, B2 and A2 high-temperature phases of Fe_2VAl. **c**,**d**, Spin-polarised electronic density of states (DOS) for the single-impurity Fe_V and V_{Fe} antisite defects and pure Fe_2VAl.

is removed due to the strong correlation of Fe−d electrons, which leads to isolated magnetic impurities in the non-magnetic, ordered host matrix. With increasing quenching temperature and thus increasing antisite concentration, the randomly distributed isolated defects form a continuum of clusters with different sizes[16,17], leading to a broadening of the localised electronic states (see Extended Data Fig.3). Eventually, a delocalised impurity band forms, i.e. the Anderson transition, as sketched in Fig.1. However, neither the CPA nor the supercell approach can determine the critical concentration for the Anderson delocalisation transition[18]. To overcome this difficulty, more effortful methods like the *typical local density of states* calculation[18] could be used as a means of possibly identifying such transitions in future works.

Magnetic properties

The formation of magnetic clusters predicted by our simulations shown in the previous section (for details see Methods) can be confirmed by our magnetisation measurements shown in Fig.3. Fig.3a exhibits the field-dependent magnetisation M at $T = 4\,\mathrm{K}$ for stoichiometric Fe_2VAl, heat-treated at different conditions. Measurements of the magnetisation have previously shown to be an effective way of probing Anderson-localised states in other semiconductors such as Si[19]. The immediate saturation of M at small fields observed in Fig.3a, the absence of hysteresis as well as the strong curvature of isothermal Arrot plots (see Extended Data Fig.7) are strong indications that the magnetic properties are dominated by the localised antisite electrons, in line with our ab initio calculations. In Fig.3b, we compare the saturation magnetisation M_{sat} of our samples with their quenching temperature T_{quench}. It can be clearly seen that M_{sat} consistently increases for higher T_{quench}, corroborating the picture drawn by our ab initio Monte-Carlo calculations. Moreover, both M_{sat} and the calculated concentration of Fe antisite defects, when rescaled to the experimental transition temperatures, increase in a similar fashion showing an abrupt increase near T_{A2}. This demonstrates that the rapid quenching method could successfully induce the magnetic antisites in these samples, which is in excellent qualitative agreement with our ab initio calculations.

Thermoelectric properties

Fig.4 shows the temperature-dependent electrical resistivity $\rho(T)$ and thermopower $S(T)$ of Fe_2VAl, measured in a wide temperature range from 4 to 800 K for samples heat-treated and quenched at various temperatures. Above $400 - 500\,\mathrm{K}$, a semiconductor-like behaviour of the resistivity, $\mathrm{d}\rho/\mathrm{d}T < 0$, is found for all samples (see Fig.4a). This can be attributed to the intrinsic pseudogap of the compound[20,21]. At lower temperatures, the behaviour modifies from semiconductor-like to metallic, $\mathrm{d}\rho/\mathrm{d}T > 0$, demonstrating the Anderson-Mott-type insulator-metal transition

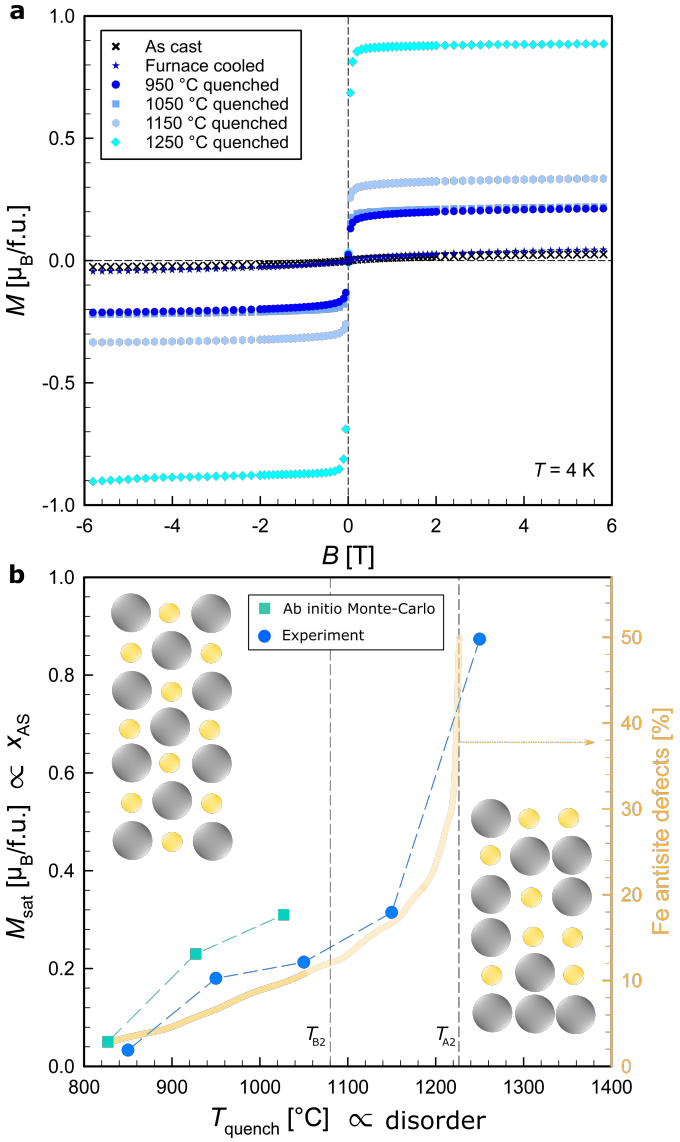

Fig. 3: **a**, Field-dependent magnetisation of Fe_2VAl at $T = 4\,\mathrm{K}$ for different quenching temperatures. **b**, Experimental and calculated saturation magnetisation versus quenching temperature. The insets show a sketch of atomic disorder, increasing with T_{quench}. Right scale shows the calculated concentration of Fe antisite defects (yellow curve) from Fig.1b, rescaled to the experimental transition temperatures T_{B2}, T_{A2} [15].

due to the delocalisation of antisite electrons with increasing T_{quench}. Indeed, the residual resistivity ρ_0 decreases by an order of magnitude with increasing T_{quench}, which also manifests itself by a substantial increase of the Hall carrier concentration (see Extended Data Fig.8a), overcompensating the increased number of scattering centres due to disorder. Furthermore, the appearance of metallic transport goes hand in hand with the development of a local maximum in $\rho(T)$ at a temperature $T_{\rho,\mathrm{max}}$, which shifts to higher temperatures as T_{quench} increases.

In Fig.4b, $S(T)$ is shown from 4 to 800 K. As-cast and furnace-cooled samples display positive values of $S(T)$ and a pronounced maximum at $\approx 200\,\mathrm{K}$, consistent with the

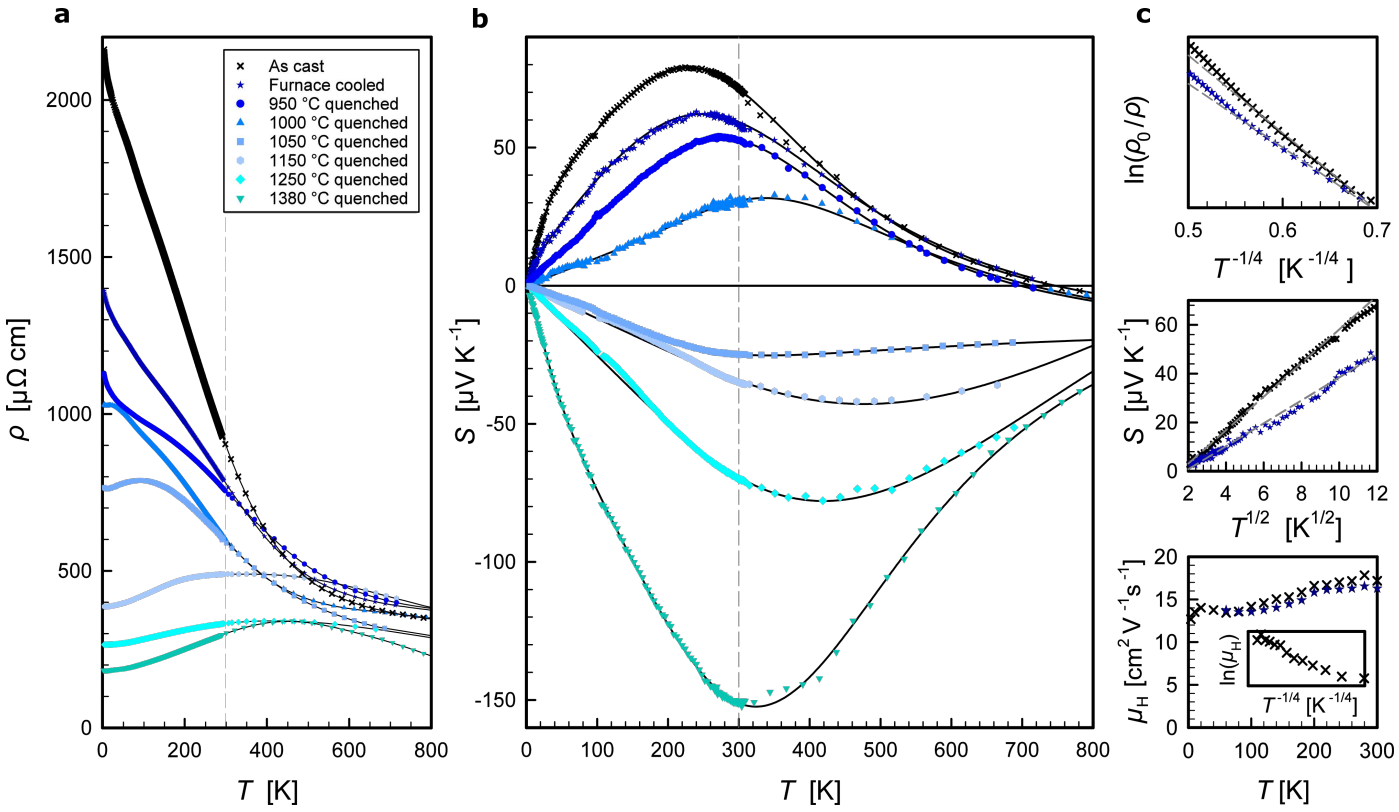

Fig. 4: **a**, Insulator-metal transition of the temperature-dependent resistivity of Fe_2VAl with increasing quenching temperature. **b**, Sign reversal of the temperature-dependent thermopower with increasing quenching temperature. Solid lines are guides to the eye. **c**, Evidence from different transport measurements for charge localisation and variable-range hopping behaviour of as-cast and furnace-cooled Fe_2VAl at low temperatures.

narrow pseudogap band structure, where E_F is situated near the valence band edge. As T_{quench} and the antisite concentration increase, $S(T)$ becomes consistently smaller at all measured temperatures and even exhibits a sign reversal for $T_{quench} > 1000\,°C$ over the whole temperature range. This implies a substantial negative contribution of the antisite electrons to $S(T)$ in order to account for the dramatic change of the thermopower, from large p-type to large n-type values.

Further evidence for the presence of Anderson-localised states near E_F is given by a more detailed analysis of the temperature-dependent transport properties. As-cast and furnace-cooled samples, according to the respective magnetic measurements, represent the dilute limit of antisites, where E_F is expected to be situated within the localised states. Indeed, the low-temperature resistivity of these samples (see upper panel Fig.4c) can be well described by phonon-assisted variable-range hopping (VRH) conduction[22]:

$$\rho(T) \propto \exp\left[\left(\frac{T_0}{T}\right)^{1/(d+1)}\right], \qquad (1)$$

which specifies in 3D to $\rho(T) \propto \exp\left[\left(\frac{T_0}{T}\right)^{1/4}\right]$, where T_0 is the characteristic Mott temperature. T_0 inversely depends on the localisation length ξ_L, which diverges at the insulator-metal transition. The fitted values of T_0 are about $2-4\,mK$, which are at least five orders of magnitude lower than for VRH between localised donor and acceptor states in marginally doped semiconductors[23,24]. Again, this low T_0 corroborates the picture of Anderson-localised states near E_F[25,26]. The temperature-dependent behaviour of the thermopower $S(T) \propto T^{1/2}$ at low temperatures (see Fig.4c centre panel) is also consistent with VRH in 3D[27], corroborating the resistivity data. Finally, even the low-temperature Hall mobility $\mu_H(T)$ shows an unusual, almost constant, slightly increasing temperature dependence (see Fig.4c lower panel), consistent with localisation of charge carriers near E_F[28]. This picture of Anderson-localised states close to the Fermi level also reconciles many other peculiar properties of this compound, e.g. metallic thermodynamic and photoemission data in spite of semiconductor-like transport properties[20], negative magnetoresistance[29], anomalous Hall effect[30] etc., which have been an ongoing discussion over the past three decades[14,20,31].

Discussion

Fig.5 shows in detail the evolution of the electronic transport across the Anderson transition as well as the enormous TE performance that can be attributed to the contribution of the delocalised impurity band. In Fig.5a we plotted the

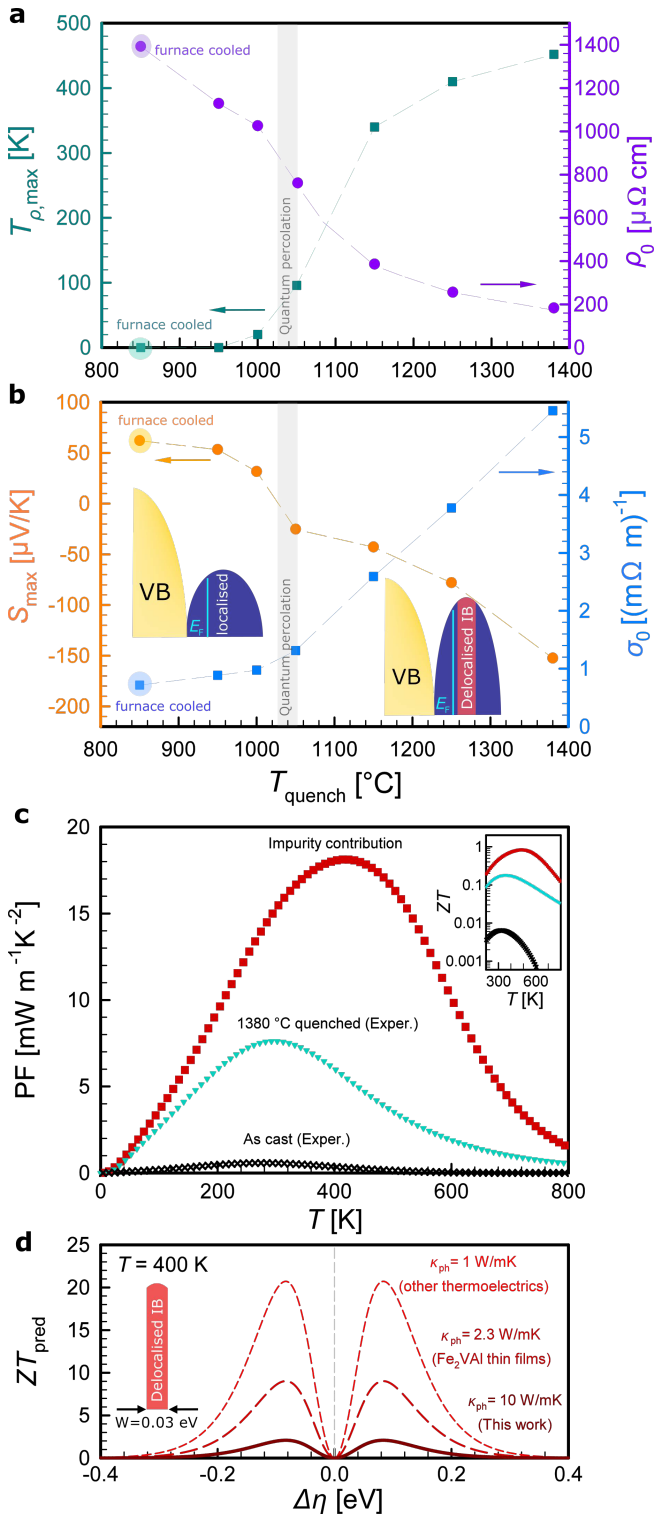

Fig. 5: **a**, Residual resistivity and temperature of the maximum of the resistivity versus quenching temperature. **b**, Peak values of the thermopower and residual conductivity versus quenching temperature. **c**, Power factor of as-cast and 1380 °C-quenched Fe_2VAl with the contribution of the impurity band (IB). The inset shows the figure of merit ZT. **d**, Predicted ZT versus reduced chemical potential relative to the centre of the impurity band. Model predictions were calculated for different values of the lattice thermal conductivity as explained in Methods.

residual resistivity ρ_0 at 4 K and $T_{\rho,\max}$ as a function of T_{quench}. With the spontaneous appearance of $T_{\rho,\max} > 0$ around $T^*_{\text{quench}} = 1000 - 1050\,^\circ$C, ρ_0 simultaneously shows a pronounced kink. In Fig.5b, we show the peak values of the thermopower $S_{\max}$ as well as the residual conductivity σ_0. Again around T^*_{quench}, $S(T)$ displays a sign reversal and σ_0 deviates from a linear scaling behaviour. These anomalies, together with the monotonous increase of $T_{\rho,\max}$ and decrease of ρ_0, clearly indicate the continous delocalisation of the impurity band (IB), as sketched in the insets of Fig.5b.

Fig.5c shows the power factor (PF) of as-cast and 1380 °C-quenched Fe_2VAl. Usually, the optimisation of thermoelectric materials involves changing the position of the Fermi level, i.e. the total number of electrons, while leaving the electronic structure unchanged, which is called rigid-band doping. Despite being undoped and not yet optimised, the maximum power factor of 1380 °C-quenched Fe_2VAl is already 7.6 mW/mK^2, which is an enhancement by an order of magnitude compared to the as-cast sample and 40% higher than the best PF for optimised rigid-band doping in this system[32]. Considering that the total thermopower S_{tot} and total conductivity σ_{tot} in a material with multiple electronic bands can be written as

$$S_{\text{tot}} = \frac{\sum_i S_i \sigma_i}{\sum_i \sigma_i}, \tag{2}$$

$$\sigma_{\text{tot}} = \sum_i \sigma_i, \tag{3}$$

with S_i, σ_i being the respective single-band contributions, we can estimate the contribution of the impurity band which led to the dramatic change in TE transport. Here, the index ($i = \{\text{pristine, impurity}\}$) refers to contributions from the pristine band structure and the delocalised impurity band. Bearing in mind that the transport properties of the as-cast sample with purely localised impurity states is mainly dominated by the pristine band structure, we can calculate the additional delocalised impurity contribution to the high-temperature-quenched samples $S_{\text{imp}}, \sigma_{\text{imp}}$ from our measured data by solving the system of Eqs.2,3. The contribution of the impurity band to the total measured power factor of the 1380 °C-quenched sample is plotted by red squares in Fig.5c. An extremely large PF of more than 18 mW/mK^2 at 400 K is found for a stoichiometric sample not yet optimally doped, exceeding that of the pristine compound by a factor of 30. It is noteworthy to mention that κ_{ph} was also reduced by a factor of $2-3$ due to the disorder introduced by quenching (see Extended Data Fig.8b). Consequently, this means that the disorder induced by thermal quenching could be a strategy that can enhance all thermoelectric properties at the same time, which is not achievable by conventional doping strategies. We expect that ZT should be further greatly enhanced by optimising the position of E_{F} and by reducing the background DOS of Fe_2VAl, which can be achieved by appropriate

co-substitutions with e.g. Si and Ta[30,32].

To make a prediction about potential ZT values in such systems near the Anderson transition, we developed a charge transport model for two mobility edges in an impurity band (see Extended Data Fig.9a). By least-squares-fitting $S(T)$ and $\rho(T)$ of 1380 °C-quenched Fe_2VAl, we found that a narrow impurity band, with a bandwidth of 0.03 eV, accounts best for the measured temperature dependencies (see Extended Data Fig.9b). The predictions of the model are shown in Fig.5d. They reveal that if the chemical potential is placed optimally near the mobility edge, a colossal $ZT > 9$ could be achieved if $\kappa_{\rm ph} \approx 2.3\,{\rm Wm^{-1}K^{-1}}$, currently achievable in Fe_2VAl by thin film deposition[33]. Considering that this strategy might be well applicable to other thermoelectric materials, which generally have even smaller values $\kappa_{\rm ph} \approx 1\,{\rm Wm^{-1}K^{-1}}$ or lower, huge values of the figure of merit $ZT \gtrsim 20$ are within reach. Such performances in terms of ZT excel those of current state-of-the-art thermoelectrics by an order of magnitude, paving the way for a paradigm shift in energy and cooling applications.

In summary, we theoretically and experimentally demonstrated how the interplay of electronic correlation, Anderson localisation and defect thermodynamics can significantly boost the TE performance in undoped bulk Fe_2VAl by passing across the Anderson transition, where electrons are delocalised but occupy only a narrow interval in energy space. Indeed, we showed that Mahan and Sofo's 'best thermoelectric' is not just a mathematical construct, but can be implemented in real materials by exploiting charge carriers at the Anderson transition in an impurity band. Moreover, controlling the level of disorder allows us to tune the optimal width of the energy-dependent transport function directly, which is not achievable by other band engineering strategies employed so far. Although disorder and charge localisation have been mostly considered as detrimental for thermoelectricity, our work discloses a novel paradigm to improve thermoelectric materials and devices via impurity conduction, employing temperature-induced disorder as a new tuning and control parameter.

[1] Seebeck, T. J. *Ueber den Magnetismus der galvanischen Kette* (1822).

[2] Champier, D. Thermoelectric generators: A review of applications. *Energy Conversion and Management* **140**, 167–181 (2017).

[3] Pourkiaei, S. M. *et al.* Thermoelectric cooler and thermoelectric generator devices: A review of present and potential applications, modeling and materials. *Energy* **186**, 115849 (2019).

[4] Mahan, G. & Sofo, J. The best thermoelectric. *Proceedings of the National Academy of Sciences* **93**, 7436–7439 (1996).

[5] Heremans, J. P., Wiendlocha, B. & Chamoire, A. M. Resonant levels in bulk thermoelectric semiconductors. *Energy & Environmental Science* **5**, 5510–5530 (2012).

[6] Mott, N. F., Pepper, M., Pollitt, S., Wallis, R. & Adkins, C. The anderson transition. *Proceedings of the Royal Society of London. A. Mathematical and Physical Sciences* **345**, 169–205 (1975).

[7] Snyder, G. J. & Toberer, E. S. Complex thermoelectric materials. *Materials for Sustainable Energy: A Collection of Peer-Reviewed Research and Review Articles from Nature Publishing Group* 101–110 (2011).

[8] Kanatzidis, M. G. Nanostructured thermoelectrics: the new paradigm? *Chemistry of Materials* **22**, 648–659 (2010).

[9] Yamamoto, K., Aharony, A., Entin-Wohlman, O. & Hatano, N. Thermoelectricity near Anderson localization transitions. *Physical Review B* **96**, 155201 (2017).

[10] Anderson, P. W. Absence of diffusion in certain random lattices. *Physical Review* **109**, 1492 (1958).

[11] Mott, N. Electrons in disordered structures. *Advances in Physics* **16**, 49–144 (1967).

[12] Hinterleitner, B. *et al.* Thermoelectric performance of a metastable thin-film Heusler alloy. *Nature* **576**, 85–90 (2019).

[13] Tsujii, N., Nishide, A., Hayakawa, J. & Mori, T. Observation of enhanced thermopower due to spin fluctuation in weak itinerant ferromagnet. *Science Advances* **5**, eaat5935 (2019).

[14] Berche, A., Noutack, M. T., Doublet, M.-L. & Jund, P. Unexpected band gap increase in the Fe_2VAl Heusler compound. *Materials Today Physics* **13**, 100203 (2020).

[15] Maier, S. *et al.* Order-disorder transitions in the Fe_2VAl Heusler alloy. *Acta Materialia* **121**, 126–136 (2016).

[16] Shklovskii, B. I. & Efros, A. L. *Electronic Properties of Doped Semiconductors*, vol. 45 (Springer Science & Business Media, 2013).

[17] Belitz, D. & Kirkpatrick, T. The Anderson-Mott transition. *Reviews of Modern Physics* **66**, 261 (1994).

[18] Dobrosavljević, V., Pastor, A. & Nikolić, B. K. Typical medium theory of Anderson localization: A local order parameter approach to strong-disorder effects. *EPL (Europhysics Letters)* **62**, 76 (2003).

[19] Mori, T., Shimazu, Y. & Ikehata, S. Magnetic susceptibility of compensated Si:P. *Solid State Communications* **91**, 13–15 (1994).

[20] Nishino, Y. *et al.* Semiconductorlike behavior of electrical resistivity in Heusler-type Fe_2VAl compound. *Physical Review Letters* **79**, 1909 (1997).

[21] Okamura, H. *et al.* Pseudogap formation in the intermetallic compounds $(Fe_{1-x}V_x)_3Al$. *Physical Review Letters* **84**, 3674 (2000).

[22] Mott, N. F. Conduction in non-crystalline materials: III. Localized states in a pseudogap and near extremities of conduction and valence bands. *Philosophical Magazine* **19**, 835–852 (1969).

[23] Prati, E., Hori, M., Guagliardo, F., Ferrari, G. & Shinada, T. Anderson–Mott transition in arrays of a few dopant atoms in a silicon transistor. *Nature nanotechnology* **7**, 443–447 (2012).

[24] Oliveira, J. F. *et al.* Pressure-induced Anderson-Mott transition in elemental tellurium. *Communications Materials* **2**, 1–10 (2021).

[25] Sefat, A. S. *et al.* Anderson-Mott transition induced by hole doping in $Nd_{1-x}TiO_3$. *Physical Review B* **74**, 104419 (2006).

[26] Ying, T. *et al.* Anderson localization of electrons in single crystals: $Li_xFe_7Se_8$. *Science Advances* **2**, e1501283 (2016).

[27] Zvyagin, I. On the theory of hopping transport in disordered semiconductors. *Physica Status Solidi (b)* **58**, 443–449 (1973).

[28] Friedman, L. & Pollak, M. The Hall effect in the variable-range-hopping regime. *Philosophical Magazine B* **44**, 487–507 (1981).

[29] Vasundhara, M., Srinivas, V. & Rao, V. Evidence for cluster glass behavior in Fe_2VAl Heusler alloys. *Physical Review B* **78**, 064401 (2008).

[30] Garmroudi, F. *et al.* Boosting the thermoelectric performance of Fe_2VAl-type Heusler compounds by band engineering. *Physical Review B* **103**, 085202 (2021).

[31] Weht, R. & Pickett, W. Excitonic correlations in the intermetallic Fe_2VAl. *Physical Review B* **58**, 6855 (1998).

[32] Kato, H., Kato, M., Nishino, Y., Mizutani, U. & Asano, S. Effect of silicon substitution on thermoelectric properties of Heusler-type Fe_2VAl alloy. *Nippon Kinzoku Gakkaishi (1952)* **65**, 652–656 (2001).

[33] Furuta, Y., Kato, K., Miyawaki, T., Asano, H. & Takeuchi, T. Fe_2VAl-based thermoelectric thin films prepared by a sputtering technique. *Journal of Electronic Materials* **43**, 2157–2164 (2014).

Supplementary Files

This is a list of supplementary files associated with this preprint. Click to download.

- MethodsXExtendeddata.pdf